MITSUBISHI ELECTRIC RESEARCH LABORATORIES
https://www.merl.com

Robust Current Fault Signature Extraction for Train Traction Motors

Liu, Dehong; Iwawaki, Tomoyuki; Hirakida, Ken; Matsui, Yoshiki; Wang, Yebin

TR2026-080 June 12, 2026

Abstract

Electrified high-speed train transportation systems utilize inverter-driven traction motors and a variable-voltage variable-frequency (VVVF) control scheme to achieve high efficiency across a wide range of speeds. However, due to the varying operating conditions, it becomes challenging to monitor the health of traction motors, especially when the train voltage and speed are unknown or not accurately measured. In this paper, we address the problem of extracting current signatures from train traction motors for fault detection without knowing the instant voltage amplitude and the instant motor speed. We propose a robust algorithm that combines minimum-variance spectral analysis to mitigate the effects of varying voltage and a speed compensation technique to tackle the varying-speed issue for extracting fault signatures in the stator current. Experimental results on different current data, including faulty laboratory motor current, onsite measurements from healthy train motors, as well as synthesized faulty train motor current, show that our method can accurately estimate the motor speed and achieve a robust spectrum under various operating conditions for fault signature extraction.

2026 IEEE Transportation Electrification Conference & Expo

Mitsubishi Electric Research Laboratories, Inc.
201 Broadway, Cambridge, Massachusetts 02139

Robust Current Fault Signature Extraction for Train Traction Motors

Dehong Liu
Mitsubishi Electric Research Laboratories
Cambridge, MA
liudh@merl.com

Tomoyuki Iwawaki
Mitsubishi Electric Corporation
Amagasaki, Japan
Iwawaki.Tomoyuki@dh.MitsubishiElectric.co.jp

Ken Hirakida
Mitsubishi Electric Corporation
Amagasaki, Japan
hirakida.ken@ak.mitsubishielectric.co.jp

Yoshiki Matsui
Mitsubishi Electric Corporation
Amagasaki, Japan
matsui.yoshiki@dh.mitsubishielectric.co.jp

Yebin Wang
Mitsubishi Electric Research Laboratories
Cambridge, MA
yebinwang@ieee.org

***Abstract*—Electrified high-speed train transportation systems utilize inverter-driven traction motors and a variable-voltage variable-frequency (VVVF) control scheme to achieve high efficiency across a wide range of speeds. However, due to the varying operating conditions, it becomes challenging to monitor the health of traction motors, especially when the train voltage and speed are unknown or not accurately measured. In this paper, we address the problem of extracting current signatures from train traction motors for fault detection without knowing the instant voltage amplitude and the instant motor speed. We propose a robust algorithm that combines minimum-variance spectral analysis to mitigate the effects of varying voltage and a speed compensation technique to tackle the varying-speed issue for extracting fault signatures in the stator current. Experimental results on different current data, including faulty laboratory motor current, onsite measurements from healthy train motors, as well as synthesized faulty train motor current, show that our method can accurately estimate the motor speed and achieve a robust spectrum under various operating conditions for fault signature extraction.**

***Index Terms*—Electrified train, Motor fault detection, VVVF operation, Spectral analysis**

I. Introduction

Electrified high-speed train transportation systems employ inverter-driven motors and a Variable Voltage Variable Frequency (VVVF) control scheme to operate efficiently across a wide range of speeds, allowing smooth acceleration, efficient cruising, and regenerative braking. For safety purposes, the online monitoring of traction motor health conditions is crucial. However, due to the varying operating conditions, it becomes challenging to extract reliable signatures from the stator current for fault detection.

For motor fault detection, a widely-used method is to use motor current signature analysis (MCSA), which extracts frequency components associated with faults such as broken rotor bars, eccentricity, and bearing defects [1]. The MCSA-based method works very well when the motor is operating at a constant speed with a constant load.

When train traction motors are operating at varying voltage and varying frequency, the current spectral analysis becomes more complicated. For example, during operations such as accelerating, braking, and running on hilly rails, etc, motor fault signature frequency and harmonic frequency components may mix together in the frequency spectrum, making it difficult to detect fault signatures. Since fault frequency components are not constant anymore, simple spectral analysis such as Fourier transform does not perform well in extracting the fault signature. Time-frequency spectrogram analysis is therefore required to capture variations of the motor speed and the current amplitude.

To tackle this challenging problem of spectral analysis under varying voltage and varying speed, many methods have been proposed to mitigate the influence of varying operating conditions. The short-time Fourier transform (STFT) is typically used to track the variation of frequency components, assuming a constant motor speed and a constant current amplitude within each short-time window. However, the spectrum of short-time window is not stable and easily affected by noise. The noise problem is then addressed in some advanced signal-processing methods, such as sparsity-driven methods [2], [3], which aim to denoise the spectrum based on the signal sparsity and smoothness property. However, these methods are not very effective for removing fixed-frequency interference. In recent years, machine learning and artificial intelligence (AI) technologies have been developed rapidly in different areas including the fault detection area [4], [5]. However, these AI-based methods typically require a large amount of training data and are difficult to generalize if not combined with the

underlying physical model.

In this paper, we focus on the time-frequency spectrogram analysis, aiming at extracting fault signatures in varying operating conditions, which is also favorable for AI-based technologies. To this end, we propose an effective method to analyze the stator current for a stable spectrogram even when the voltage amplitude and the motor speed are unknown. Considering the VVVF operation of traction motors in high-speed trains, we first employ minimum-variance (MV) spectral analysis [6] to achieve MV spectrogram by suppressing the noise of STFT spectrogram. Then the motor speed is estimated by analyzing the relationship between two consecutive time window spectra in the MV spectrogram. The dominant frequency spectrum is then extracted from the compensated spectrogram using the principal component analysis. Experiments conducted on a laboratory motor and a train traction motor show that our method can accurately estimate the motor speed and achieve high-precision spectrum analysis.

II. Motor Current Signature

A. Constant-speed operation

Let f_s be the fundamental frequency of the PWM inverter's output voltage. The motor current frequency components include the fundamental operating frequency component and its harmonics under normal healthy conditions. The time-domain stator current can be formulated as

$$i_h(t) = \sum_n I_{s,n} \cos(2\pi f_{s,n} t + \phi_{s,n}), \tag{1}$$

where $I_{s,1}$ is the current amplitude of operating frequency $f_{s,1} = f_s$; ϕ_s is the initial phase of the operating frequency component; subscript $n (n \geq 2)$ represents the order of harmonics; and $f_{s,n} = nf_s$.

In the event of a motor fault, additional fault frequency components will be induced in the stator current

$$i_f(t) = i_h(t) + \sum_l I_{f,l} \cos(2\pi f_{f,l} t + \phi_{f,l}), \tag{2}$$

where $I_{f,l}$ represents the amplitude of the lth fault frequency component $f_{f,l}$, and $\phi_{f,l}$ is the initial phase of the lth fault frequency component.

Extensive research has been conducted in identifying the fault frequency based on different physical models. For example, when a broken rotor bar fault occurs in a squirrel-cage induction motor, the fault frequency can be expressed as [7]

$$f_{bar} = (1 \pm 2\tau s) f_s, \tag{3}$$

where $\tau = 1, 2, \ldots$, and s is the motor slip, which can be calculated using the motor n_r and the synchronous speed n_s as $s = 1 - \frac{n_r}{n_s}$.

For bearing faults, depending on the fault location in the bearing and the bearing size, the characteristic fault frequency induced in the stator current is proportional to the mechanical frequency of the rotor, *i.e.* [8]

$$f_b \propto f_r = \frac{1-s}{p} f_s. \tag{4}$$

For eccentricity fault in most induction machines, it can be identified using slot harmonics in the current [9], [10]

$$f_{slt} = ((\kappa Z \pm n_d)\frac{1-s}{p} + \nu) f_s, \tag{5}$$

where Z is the number of rotor slots; p is the number of pole pairs; $\kappa = 1, 2, 3, ...$; n_d is the eccentricity order ($n_d = 0$ in case of static eccentricity and $n_d = 1, 2, 3, ...$, in case of dynamic eccentricity); and $\nu = \pm 1, \pm 3, \pm 5, ...$ is the order of stator time harmonics.

When the motor is operating at a constant speed and a constant load, all these fault frequencies are of fixed values. Fourier spectrum analysis can then be applied directly to extract fault frequency components for fault detection.

B. Varying operating conditions

For inverter-drive traction motors in the high-speed train, variable voltage variable frequency control scheme is adopted to achieve high efficiency while the train is operating at a wide range of speed. In such situations, the current magnitude $I_{s,1}$ and the operating frequency f_s are time-varying. Therefore, it is challenging to analyze the frequency spectrum for fault detection and harmonic analysis.

Fig. 1(a) and Fig. 1(b) show representative time-domain waveforms in different time scales. In particular, Fig. 1(a) plots the stator current of 24 second when the train is running at braking mode, with a slowing-down speed. We observe that the amplitude of stator current decreases at different stages to meet the load requirement. In Fig. 1(b), we zoom in the time scale to check the waveform of several periods. We observe that the time-domain current is not a purely sinusoidal signal, but contains significant harmonic components caused by the inverter and other interference sources.

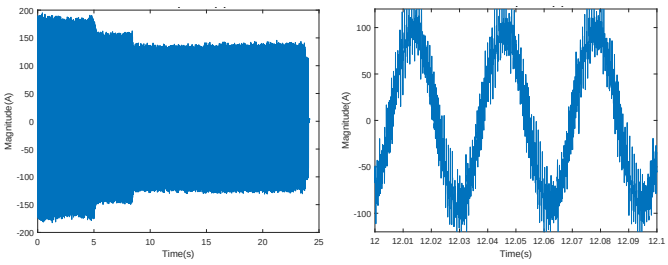

(a) (b)

Fig. 1. Time-domain stator current in varying operating condition of different time windows.

To further analyze the harmonic frequency components, we use Fourier transform to perform spectral analysis. We perform Fourier transform on the 24 s current signal, with spectrum shown in Fig. 2(a). First, from the Fourier spectrum, we observe that the operating frequency spans a frequency range from 20 Hz to 52 Hz. This is because under VVVF control, the train speed is proportional to the inverter's output frequency. In this case, the train speed is reduced by decreasing the inverter output frequency accordingly. Second, from the Fourier spectrum, we do not clearly observe harmonic frequency components, although the time-domain current signal

in Fig. 1(b) shows strong harmonic patterns. This is because the harmonic frequency components of different orders are mixed together due to the varying operating frequency. Therefore, it is not feasible to extract the harmonic and fault frequency components for further analysis using conventional Fourier transform. To better resolve frequency components, we consider a shorter-time window, for which the motor speed can be treated as a constant. Fig. 2(b) presents frequency spectra using 2.5-second time windows. We can observe that although the operating frequency can be well resolved, the visibility of harmonic and fault frequency components is not stable due to the varying-speed operation. The harmonic frequency components may or may not be detectable, as indicated by the black solid line and the red dash line, depending on the selected time window.

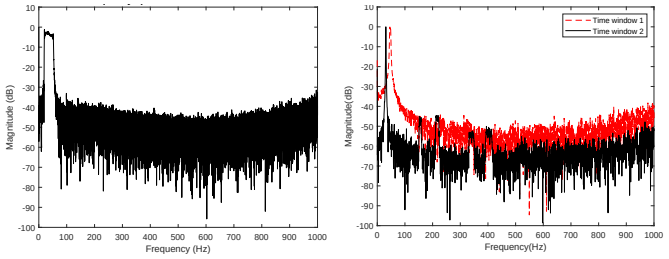

(a) (b)

Fig. 2. Frequency spectra of stator current in varying operating condition using Fourier transform with (a) 24 second time window measurements and (b) 2.5 second time window measurements.

III. Proposed Method

Under the VVVF control, the amplitude and the frequency of the stator current vary to meet the load change and the speed change. We first employ minimum-variance (MV) spectral analysis to deal with the amplitude variation [6], and then estimate the motor speed from the MV spectrum. The final equivalent spectrum is extracted from speed-compensated MV spectrum using singular value decomposition. The proposed algorithm is described as follows.

A. Minimum-variance-based spectral analysis

To capture the time-varying frequency components, short-time Fourier transform (STFT) is typically used for spectral analysis, assuming that the motor speed remains constant in the short-time window used for spectral analysis. Let $\{i_1(\tau), i_2(\tau), ..., i_n(\tau), ..., i_N(\tau)\}$ be N current segments by putting a sliding time window on the measured current $i(t)$, where the n^{th} segment $i_n(\tau)$ can be expressed as

$$i_n(\tau) = i(\tau + (n-1)t_s), \quad \text{for } \tau = [0, \Delta t, ..., t_w],\ n = 1, ..., N, \tag{6}$$

where Δt is the sampling time, t_w is the window size in time, t_s is the time step between two consecutive time windows, and we have $t_s < t_w$ for overlapped windows. Both t_w and t_s are multiples of Δt. The STFT spectrogram is obtained by using FFT on each short-time window signal, i.e.,

$$\hat{S}_n^{FT}(\omega) \triangleq I_n(\omega) = FFT(i_n(\tau)). \tag{7}$$

To improve spectrogram quality, we employ a minimum-variance-based method to address magnitude variations and noise [6]. In particular, we consider a refined time step of sliding windows $t_{MV} = \frac{t_s}{M}$, then each STFT time window signal $i_n(\tau)$ corresponds to M consecutive time windows $i_{n,m}(\tau)$, for $m = 1, ..., M$, of the same length in the MV spectrum analysis. The spectra of the M consecutive time windows are then combined, after proper phase alignment, using optimized frequency-dependent weights as

$$\hat{S}_n^{MV}(\omega) = \sum_{m=1}^{M} \beta_{n,m}(\omega) I_{n,m}(\omega) e^{-j\omega(m-1)t_{MV}}, \tag{8}$$

where the weight $\beta_{n,m}(\omega)$ is optimized by minimizing the noise variance of spectrum at each frequency ω, i.e.,

$$\min_{\beta_{n,m}} \sum_{m} |\beta_{n,m}(\omega) I_{n,m}(\omega) e^{-j\omega(m-1)t_{MV}}|^2, \quad s.t. \quad \sum_{m} \beta_{n,m}(\omega) = 1. \tag{9}$$

Let $\beta_n = [\beta_{n,1}(\omega), ..., \beta_{n,m}(\omega), ..., \beta_{n,M}(\omega)]^T \in \mathcal{R}^{M\times 1}$, $\mathbf{R}_n = diag\{I_{n,1}^2(\omega), ..., I_{n,m}^2(\omega), ..., I_{n,M}^2(\omega)\} \in \mathcal{R}^{M\times M}$, and $\mathbf{a} = [1, ..., 1, ..., 1]^T \in \mathcal{R}^{M\times 1}$.

The closed-form solution of (9) is given by

$$\beta_n = \frac{\mathbf{R}_n^{-1}\mathbf{a}}{\mathbf{a}^T\mathbf{R}_n^{-1}\mathbf{a}}. \tag{10}$$

In our experiments, considering the frequency resolution requirement, we set the time window duration of each segment as $t_w = 2$s, the time step between two consecutive time windows as $t_s = 2$s, then the total number of current segments N is determined according to the total length of measurements. A total of $M = 8$ consecutive window Fourier spectra are combined to form one MV spectrum according to (8).

B. Speed estimation

Let $f_n = \alpha_n f_{ref}$ be the operating frequency of the n^{th} time window, where α_n is a scaling factor of the n^{th} time window and f_{ref} is the reference frequency. Under the VVVF control, the motor speed during the n^{th} time window can be expressed as $v_n = \alpha_n v_{ref}$, where v_{ref} is the reference speed. Although in theory α_n can be estimated by the operating frequency, the accuracy of the speed estimation is poor. This is because the frequency resolution is restricted by the time window length, *i.e.*, $\Delta f = \frac{1}{t_s}$. In practice, when the speed change is small, the operating frequency variation may be smaller than $\Delta f/2$, resulting in the same discretized operating frequency in the spectrum. To improve the estimation accuracy, we take into account high-order harmonics for speed estimation. The scaling factor α_n is achieved by

$$\hat{\alpha}_n = \text{argmax}_{\alpha_n} |\hat{S}_{ref}^{MV}(\omega)|^T |\hat{S}_n^{MV}(\frac{1}{\alpha_n}\omega)|, \tag{11}$$

where $\hat{S}_{ref}^{MV}(\omega)$ is the MV spectrum at the reference speed, and $\hat{S}_n^{MV}(\frac{1}{\alpha_n}\omega)$ is a scaled version of the MV spectrum corresponding to the n^{th} time window. Note that in this cross-correlation computation in (11), we only consider the magnitude, not the phase of the spectrum.

If we take the average of rotor speed as the reference for speed normalization, *i.e.*, $v_{ref} = \frac{1}{N}\sum_{n=1}^{N} v_n$, then the scaling factor is the normalized speed. The average of scaling factors is

$$\frac{1}{N}\sum_{n=1}^{N}\hat{\alpha}_n = \frac{1}{N}\sum_{n=1}^{N}\frac{v_n}{v_{ref}} = 1. \tag{12}$$

To start speed estimation without knowing the average rotor speed, we use the first time window spectrum as reference to calculate

$$\begin{aligned}\alpha'_n =& \text{argmax}_{\alpha'_n}|\hat{S}_1^{MV}(\omega)|^T|\hat{S}_n^{MV}(\frac{1}{\alpha'_n}\omega)|,\\ \text{s.t. } & |\frac{\alpha'_n}{\alpha'_{n-1}} - 1| < \frac{f_{ref}}{f_{max}}, \text{for } n = 1, 2, ..., N.\end{aligned} \tag{13}$$

It is clear that we have $\alpha'_1 = 1$. After getting all $\alpha'_n (n = 1, ..., N)$, the scaling factor satisfying (12) can be computed as

$$\hat{\alpha}_n = \frac{\alpha'_n}{\frac{1}{N}\sum_{n'=1}^{N}\alpha'_{n'}}. \tag{14}$$

C. Speed compensation

To compensate the impact of speed, one way is to add scaled short-time window spectra together, with well aligned magnitude according to (11). However, the impact of speed on current phase of each time window is still not well compensated. To further improve the performance, we compensate the impact of speed by resampling the stator current according to the rotor angle such that current phase is also well aligned. The details of speed compensation are described as follows. Once we have an estimated scaling factor (normalized speed) for each time window, we upsample the normalized speed from time step t_s to time step Δt using linear interpolation according to

$$\{\tilde{\alpha}_k | t_k = (k-1)\Delta t\} = Interp\{\hat{\alpha}_n | t_n = \frac{t_w}{2} + (n-1)t_s\}. \tag{15}$$

The rotor angle position (without phase unwrapping) corresponding to stator current samples can be calculated as

$$\theta_k = \sum_k \frac{2\pi\tilde{\alpha}_k v_{ref}\Delta_t}{60}. \tag{16}$$

Time-domain current is then resampled uniformly in the spatial rotor angle as

$$\begin{aligned}&\{\tilde{i}(\theta'_k)|\theta'_k = \frac{2\pi v_{ref} k\Delta_t}{60}\} =\\ &Interp\{i[(k-1)\Delta_t] = i(\theta_k)|\theta_k = \sum_k \frac{2\pi\tilde{\alpha}_k v_{ref}\Delta_t}{60}\}.\end{aligned} \tag{17}$$

The resampled stator current $\tilde{i}(\theta'_k)$ is equivalent to the current at constant-speed operation.

D. Frequency component extraction

After speed compensation, the resampled stator has a constant operating frequency. However, due to the VVVF control, the amplitude of the stator current may still vary because of the load change. Here we employ the minimum-variance-based spectral analysis again to deal with the amplitude variation [6], and use the principal component analysis (PCA) method to extract the dominant spectrum of the compensated MV spectrogram as the final spectrum. Let $\bar{\mathbf{I}}_{MV}$ be the MV spectrogram of speed-compensated stator current. We perform singular value decomposition (SVD) on $\bar{\mathbf{I}}_{MV}$

$$\bar{\mathbf{I}}_{MV} = \mathbf{U}\mathbf{\Sigma}\mathbf{V}^\top = \sum_j \sigma_j \mathbf{u}_j \mathbf{v}_j^\top. \tag{18}$$

We take $\mathbf{u}_1$ as the speed-independent frequency component of stator current. Since this spectrum is speed-independent and with a fixed fault frequency component to operating frequency component ratio, it is robust for motor fault detection and severity estimation.

IV. Experiments

A. Experiment setup

To monitor the health condition of train traction motors, it is necessary to collect real-time motor current for analysis. However, since safety is our first priority in experiments, a faulty motor is never intentionally used on an in-service train to implement experiments. Therefore, we only have access to stator current measurements from healthy traction motors on a train during its regular operations, which include all kinds of speed patterns.

For faulty data, instead of collecting on a train traction motor, we collect real-time stator current on a laboratory motor, which is of the same type used in the train but with some controllable faults for experimental study. To generate faulty conditions, we apply an unbalanced torque on the rotor of the laboratory motor to mimic unbalanced load operations and collect its real-time stator current. Fig. 3 shows an illustration diagram of the experimental setup in lab.

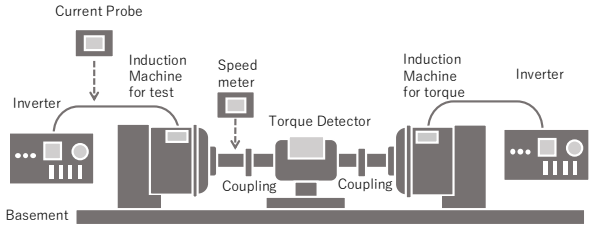

Fig. 3. Experimental setup.

B. Results of current signature analysis

1) Current of laboratory faulty motor: An example of the time-domain stator current of the motor operating at constant-speed condition is shown in Fig. 4 (a), where we record about 31 s time-domain data with a sampling rate of 5 kHz. We plot its Fourier spectrum of frequency from zero to 1

kHz in Fig. 4 (b). Since the motor operates under steady conditions with a constant speed, the frequency spectrum shows the operating frequency component, its harmonics, and fault signatures caused by imbalance appear as sidebands at approximately 0.5× and 1.5× the operating frequency.

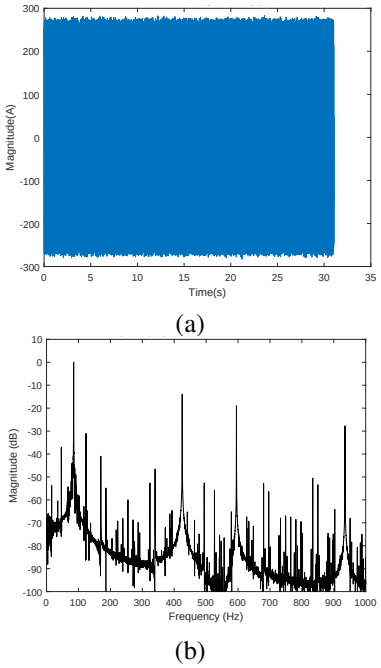

Fig. 4. Time-domain current of laboratory motor and its frequency spectrum using FFT.

2) Current of healthy train motor: An example of the time-domain stator current of the train motor operating at varying-speed condition is shown in Fig. 5(a), where we record approximately 80 s long with a sampling rate of 24 kHz. We plot its Fourier spectrum of frequency from zero to 2 kHz in Fig. 5(b). Due to the speed variation, the harmonics and fault signatures are not clear for further analysis. By analyzing the scaling factor of MV spectrogram, the normalized speed is shown in Fig. 6(a), from which we can see the estimated speed (red line) is very well aligned with measured speed (blue line). Due to the low resolution of the A/D converter, the measured speed shows some quantization error. With speed compensation, the frequency spectrum using our proposed method is shown in Fig. 6(b), where we observe clearly the operating frequency component and its harmonics. Since the motor is healthy, no fault signature is observed.

3) Synthesized current of faulty train motor: An example of synthesized time-domain stator current of the train motor operating at varying-speed condition is shown in Fig. 7(a), where we modulate the stator current of a faulty laboratory motor using the amplitude profile of a healthy train traction motor (the same amplitude profile shown in Fig. 1) during its braking procedure, and then resample it at non-uniform rotor position angle according to the instant rotor speed. The synthesized current is about 80 s long with a sampling rate of 24 kHz. We plot its Fourier spectrum of frequency from zero to

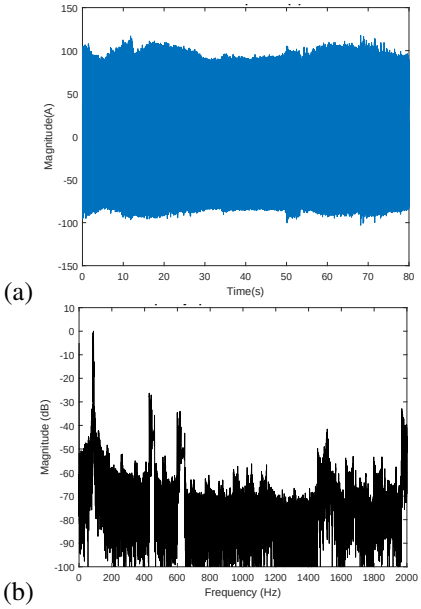

Fig. 5. Time-domain current of train motor and its frequency spectrum using FFT.

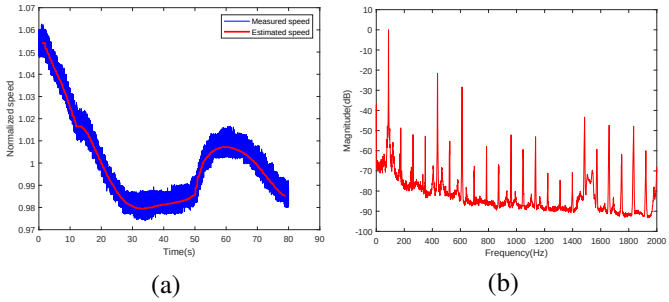

Fig. 6. (a) Estimated speed versus measured speed using a low-bit AD converter. (b) Current spectrum after speed compensation.

2 kHz in Fig. 7(b). Due to the speed variation, the harmonics and fault signatures are not detectable for further analysis. Using our proposed method, the initial STFT spectrogram shown in Fig. 8(a) appears relatively noisy. The denoised MV spectrogram is shown in Fig. 8(b), with the signal-to-noise ratio much improved. If PCA is applied to the denoised MV spectrogram, the resulting spectrum is shown in Fig. 8(c). We observe that fault signatures of imbalance, i.e., sideband frequency components at approximately 0.5× and 1.5× the operating frequency, cannot be resolved. With proper speed compensation using our proposed method, the final dominant spectrum using PCA is shown in Fig. 8(d), where we can clearly see fault signatures and harmonics.

Regarding computational time, processing an 80 s current signal takes approximately 76 s on a Windows machine equipped with an Intel Core i7-14700 (2.0 GHz) CPU and 64 GB RAM using MATLAB R2024b. This includes data loading, STFT spectrogram generation, MV spectrogram computation, speed estimation and compensation, final speed-independent spectrum extraction, and result visualization. The processing time is comparable to the signal duration, demonstrating the

feasibility of near real-time implementation.

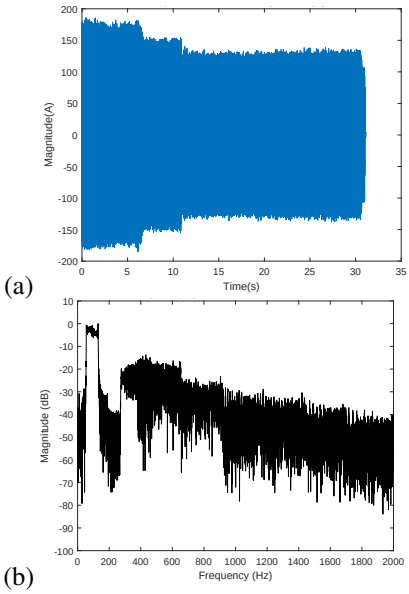

Fig. 7. (a) Synthesized time-domain current of faulty train motor, and (b) Corresponding frequency spectrum of the time-domain current using FFT.

V. Conclusion

In this paper, we address the problem of extracting current signatures for fault detection in train motors under the VVVF control, despite the unknown varying motor speed and the unknown varying voltage amplitude. We propose a robust algorithm for fault signature extraction based on speed estimation using denoised spectrogram of the stator current. With proper speed compensation, fault signatures and harmonics can then be identified in the principal component of the speed-compensated spectrogram. Experimental results on motor current data, including laboratory motor current, onsite train motor current, and synthesized faulty train motor current, show that our method can accurately estimate the motor speed and achieve a robust spectrum by compensating the impact of the motor speed. Frequency components with magnitudes up to 50 dB below the operating signal can now be extracted effectively for further fault detection and harmonic analysis.

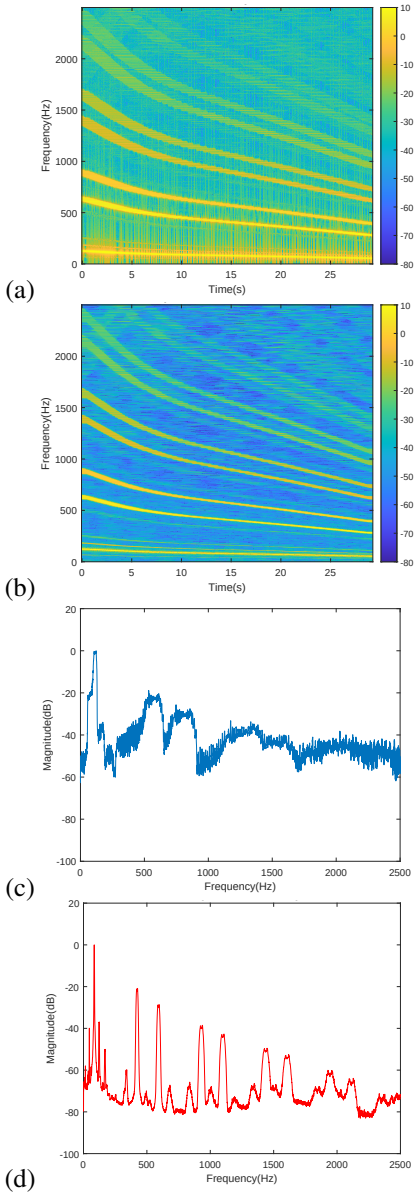

Fig. 8. (a) STFT spectrogram of synthesized stator current of faulty train motor, (b) MV spectrogram of synthesized stator current of faulty train motor, (c) dominant frequency spectrum without speed compensation, and (d) dominant frequency spectrum after speed compensation using our proposed method.

References

[1] W. T. Thomson and M. Fenger, "Current signature analysis to detect induction motor faults," *IEEE Industry Applications Magazine*, vol. 7, no. 4, pp. 26–34, 2001.

[2] D. Liu and D. Lu, "Off-the-grid compressive sensing for broken-rotor-bar fault detection in squirrel-cage induction motors," *IFAC-PapersOnLine*, vol. 48, no. 21, pp. 1451–1456, 2015.

[3] D. Liu, A. Varatharajan, and A. Goldsmith, "Extracting broken-rotor-bar fault signature of varying-speed induction motors," in *Proceedings of the Asia Pacific Conference of the PHM Society*, vol. 4, 2023.

[4] M. Z. Ali, M. N. S. K. Shabbir, S. M. K. Zaman, and X. Liang, "Single-and multi-fault diagnosis using machine learning for variable frequency drive-fed induction motors," *IEEE Transactions on Industry Applications*, vol. 56, no. 3, pp. 2324–2337, 2020.

[5] I. Martin-Diaz, D. Morinigo-Sotelo, O. Duque-Perez, and R. J. Romero-Troncoso, "An experimental comparative evaluation of machine learning techniques for motor fault diagnosis under various operating conditions," *IEEE Transactions on Industry Applications*, vol. 54, no. 3, pp. 2215–2224, 2018.

[6] D. Liu, H. Inoue, and M. Kanemaru, "Robust motor current signature analysis (mcsa)-based fault detection under varying operating conditions," in *2022 25th International Conference on Electrical Machines and Systems (ICEMS)*. IEEE, 2022.

[7] F. Filippetti, G. Franceschini, C. Tassoni, and P. Vas, "AI techniques in induction machines diagnosis including the speed ripple effect," *IEEE Transactions on Industry Applications*, vol. 34, no. 1, pp. 98–108, 1998.

[8] S. Zhang, B. Wang, M. Kanemaru, C. Lin, D. Liu, M. Miyoshi, K. H. Teo, and T. G. Habetler, "Model-based analysis and quantification of bearing faults in induction machines," *IEEE Transactions on Industry Applications*, vol. 56, no. 3, pp. 2158–2170, 2020.

[9] P. Vas, *Parameter estimation, condition monitoring, and diagnosis of electrical machines*. Oxford University Press, 1993, vol. 27.

[10] K. D. Hurst and T. G. Habetler, "Sensorless speed measurement using current harmonic spectral estimation in induction machine drives," *IEEE Transactions on Power Electronics*, vol. 11, no. 1, pp. 66–73, 1996.